Quantum phase-space picture of Bose-Einstein condensates in a double well

Khan W. Mahmud,[1,*] Heidi Perry,[2,†] and William P. Reinhardt[1,2]
[1]*Department of Physics, University of Washington, Seattle, Washington 98195-1560, USA*
[2]*Department of Chemistry, University of Washington, Seattle, Washington 98195-1700, USA*
(Received 29 November 2003; revised manuscript received 30 November 2004; published 28 February 2005)

We present a quantum phase-space model of the Bose-Einstein condensate (BEC) in a double-well potential. In a quantum two-mode approximation we examine the eigenvectors and eigenvalues and find that the energy correlation diagram indicates a transition from a delocalized to a fragmented regime. Phase-space information is extracted from the stationary quantum states using the Husimi distribution function. We show that the mean-field phase-space characteristics of a nonrigid physical pendulum arises from the exact quantum states, and that only 4–8 particles per well are needed to reach the semiclassical limit. For a driven double-well BEC, we show that the classical chaotic dynamics is manifest in the dynamics of the quantum states. Phase-space analogy also suggests that a π phase-displaced wave packet put on the unstable fixed point on a separatrix bifurcates to create a superposition of two pendulum rotor states—a macroscopic superposition state of BEC. We show that the choice of initial barrier height and ramping, following a π phase imprinting on the condensate, can be used to generate controlled entangled number states with tunable extremity and sharpness.

DOI: 10.1103/PhysRevA.71.023615 PACS number(s): 03.75.Lm, 03.75.Gg, 03.65.Sq

I. INTRODUCTION

Although the Bose-Einstein condensate (BEC) is well described by mean-field theory [1], it has many aspects that can only be described in a quantum picture containing a proper description of correlations. Examples include number squeezing [2] and the superfluid to Mott insulator transition [3] observed recently in optical lattices. The essential underlying physics can be understood with the study of a simpler double-well BEC with a variable barrier height in the well-known quantum two-mode approximation [4,5]. Quantum fluids in a double-well potential exhibit many rich phenomena related to the coherence, e.g., the Josephson effect [6] and the de Broglie wave interference [7]. A mean-field description, although appropriate in explaining these "Josephson-related effects," cannot describe the "number-squeezing effects" described earlier. In this paper we develop a quantum phase-space picture of BEC in a double well and study the connection between the mean-field and quantum effects. As important applications of our model, we investigate dynamics in phase space, study quantum manifestations of classical chaos in a driven double well, and show dynamic generation of tunable entangled number states with well-defined and controlled entanglement.

It was long ago noted by Anderson [8] that the Josephson effect, namely, two quantum fluids connected by a tunnel junction [9], may be modeled as a physical pendulum. Similarly, Smerzi *et al.* in Ref. [10] showed that the semiclassical (large N) dynamics of two weakly linked BECs can be modeled as a classical nonrigid physical pendulum. We begin, here, with the full quantum-mechanical description of a double-well BEC in a two-mode approximation [4,5,11], and show that the mean-field semiclassical limit of a nonrigid physical pendulum emerges from the exact quantum treatment. By treating the phase and the number difference of the condensates in two wells as conjugate variables, phase-space information is extracted from the exact (two-mode) quantum wave function using the Husimi projection [12] of semiclassical quantum mechanics. We show that these phase-space projections of exact quantum eigenstates are localized on the known classical energy contours of the nonrigid physical pendulum [10], and thus the mean-field classical phase-space properties, such as libration and π states, are seen to be a property of the exact quantum eigenstates. We explore quantum classical correspondence for the stationary states in phase space as a function of particle number and show that the semiclassical limit already emerges for particle numbers as small as 4–8 per well.

The quantum phase-space model also reveals an underlying time-dependent semiclassical dynamics in phase space. In a study of the dynamics of a displaced coherent state, we show a surprisingly close correspondence between classical whorls and quantum dynamics even for N as small as four per well. We further illustrate that a sinusoidally driven double-well BEC (a driven physical pendulum) shows clear signatures of classical chaos in the quantum phase space. This can be contrasted with a different property of a chaotic system—the recently observed phenomenon of dynamical tunneling [13,14], which is a quantum motion between two resonance zones in phase space not allowed within the classical dynamics. We also discuss the dynamics of a coherent ground state after a sudden change of barrier height [2,15]. We show that the oscillations between a number-squeezed and a phase-squeezed state is a rotation of a pulsing ellipse in the phase space.

Due to the macroscopic nature of its wave function, BEC should be an ideal system for the generation of macroscopic quantum superposition states (Schrödinger cat states). The creation of macroscopic superposition states in various

*Present address: Department of Physics, University of Michigan, Ann Arbor, MI 48109, USA.
†Present address: Department of Chemistry, Columbia University, New York, NY 10027, USA.

condensed-matter systems has received attention [16]. In the context of BEC, several authors have suggested producing such states [17–20], although none have been demonstrated experimentally. We show how such macroscopic quantum superposition states are generated in phase space with a single-component BEC in a double well. Starting with a ground state centered at the origin and displacing it through a π phase imprinting to put it on the hyperbolic fixed point of the classical phase space, the autonomous dynamics splits the wave packet along the separatrix to create entangled number states of the form

$$|\Psi\rangle = \frac{1}{\sqrt{2}}(|n_L, N-n_L\rangle + |N-n_L, n_L\rangle), \tag{1}$$

where $|n_L, n_R\rangle$ denotes a state with n_L particles in the left well, n_R in the right well, and $N=n_L+n_R$. The idea of the exploitation of unstable fixed points to generate such entangled states with BEC in a double well and two-component condensates in a single trap has also been discussed in the works of Polkovnikov *et al.* [19] and Micheli *et al.* [20], a discussion of which is given in Sec. V. Unlike in other proposals [17,19,20], we use the barrier height to control the squeezing of the initial BEC ground state, followed by a continuous change of barrier height to control both the extremity (the value of n_L) and the sharpness (the spread around n_L) of the final entangled state. A very simple particle-loss scheme [18] is used here to test the robustness of the entangled states.

The paper is organized as follows. In Sec. II we introduce the model Hamiltonian and examine its ground and excited states. In Sec. III we find the Husimi probablity distribution function for the quantum states, show that the quantum states are localized on the classical phase-space orbits of a known nonrigid physical pendulum. In Sec. IV we analyze phase-space dynamics for a displaced wave packet, study chaotic dynamics of a driven double well, and explain phase-space rotation of a ground state. In Sec. V we provide a phase-space analysis of the generation of tunable entangled states. Remarks and a summary in Sec. VI conclude the paper.

II. QUANTUM TWO-STATE MODEL

A. Model Hamiltonian

The many-body Hamiltonian for a system of N weakly interacting bosons in an external potential $V(\mathbf{r})$, in second quantization, is given by

$$\hat{H} = \int d\mathbf{r}\hat{\Psi}^\dagger(\mathbf{r})\left[-\frac{\hbar^2}{2m}\nabla^2 + V(\mathbf{r})\right]\hat{\Psi}(\mathbf{r}) + \frac{g}{2}\int d\mathbf{r}\hat{\Psi}^\dagger(\mathbf{r})\hat{\Psi}^\dagger(\mathbf{r})\hat{\Psi}(\mathbf{r})\hat{\Psi}(\mathbf{r}), \tag{2}$$

where $\hat{\Psi}(\mathbf{r})$ and $\hat{\Psi}^\dagger(\mathbf{r})$ are the bosonic annihilation and creation field operators, m is the particle mass, and $g=(4\pi a_s\hbar^2)/m$, where a_s is the s-wave scattering length.

In studies of double-well BEC or two-component condensates, the low-energy many-body Hamiltonian in Eq. (2) can be simplified in the well-known two-mode approximation [4,5]. Many authors have studied the double-well condensate using the two-mode approximation. We use the model introduced by Spekkens and Sipe [5]. The exclusion of the nonlinear tunneling terms in this model gives rise to the Bose-Hubbard model [21]. The full two-mode Hamiltonian is

$$\hat{H} = \epsilon_{LL}\hat{N}_L + \epsilon_{RR}\hat{N}_R + [\epsilon_{LR} + gT_1(\hat{N}-1)](a_L^\dagger a_R + a_R^\dagger a_L) + \frac{gT_0}{2}(\hat{N}_L^2 + \hat{N}_R^2 - \hat{N}) + \frac{gT_2}{2}(a_L^\dagger a_L^\dagger a_R a_R + a_R^\dagger a_R^\dagger a_L a_L + 4\hat{N}_L\hat{N}_R), \tag{3}$$

where $\hat{N}_L=a_L^\dagger a_L$, $\hat{N}_R=a_R^\dagger a_R$, $\hat{N}=\hat{N}_L+\hat{N}_R$, and

$$\epsilon_{ij} = \int d\mathbf{r}\phi_i(\mathbf{r})\left(-\frac{\hbar^2}{2m}\nabla^2 + V(\mathbf{r})\right)\phi_j(\mathbf{r}), \tag{4}$$

where $i,j=L,R$,

$$T_0 = \int d\mathbf{r}\phi_L^4(\mathbf{r});\ T_1 = \int d\mathbf{r}\phi_L^3(\mathbf{r})\phi_R(\mathbf{r});$$

$$T_2 = \int d\mathbf{r}\phi_L^2(\mathbf{r})\phi_R^2. \tag{5}$$

Here ϕ_L and ϕ_R are the left and right localized single-particle Schrödinger wave functions, the ϵ_{LL} and ϵ_{RR} are the energies of a single particle in the left and right wells, ϵ_{LR} is the single-particle tunneling amplitude; T_0 is the mean-field energy in each well and $T_{1,2}$ are nonlinear tunneling matrix elements.

We make a one-parameter approximation [11] of the single-particle energies and the tunneling matrix elements

$$g=1, \quad \epsilon_{LL}=\epsilon_{RR}=T_0=1, \quad \epsilon_{LR}=T_1=-e^{-\alpha},$$

$$T_2=-e^{-2\alpha}. \tag{6}$$

This parametrization allows a simple study of continuous change in the linear and nonlinear tunneling through variation of a single parameter α. In our computations with this model we ignore the T_2 term, which scales as $\exp(-2\alpha)$. The model Hamiltonian then reduces to

$$\hat{H} = \epsilon_{LL}\hat{N}_L + \epsilon_{RR}\hat{N}_R + [\epsilon_{LR} + gT_1(\hat{N}-1)](a_L^\dagger a_R + a_R^\dagger a_L) + \frac{gT_0}{2}(\hat{N}_L^2 + \hat{N}_R^2 - \hat{N}). \tag{7}$$

B. Fock-state analysis

The most general state vector is a superposition of all the number states

$$|\Psi\rangle = \sum_{n_L=0}^{N} c_{n_L}^{(i)}|n_L, N-n_L\rangle, \tag{8}$$

where

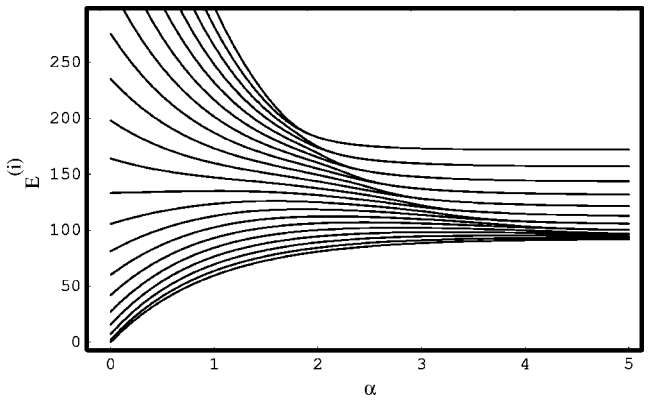

FIG. 1. Energy correlation diagram for 20 particles showing the eigenvalues as a function of barrier height α. Note the merging of energy levels as tunneling decreases.

$$|n_L, N-n_L\rangle = \frac{(a_L^\dagger)^{n_L}}{\sqrt{n_L!}} \frac{(a_R^\dagger)^{n_R}}{\sqrt{(N-n_L)!}} |vac\rangle. \tag{9}$$

Finding the eigenvalues and eigenvectors of the model Hamiltonian in the Fock basis can be easily accomplished by diagonalizing a $(N+1)\times(N+1)$ tridiagonal matrix.

Authors in Ref. [5] studied condensate fragmentation by looking at the ground state as the barrier is raised. We extend their analysis to look at the coefficients of the higher-lying states and examine the energy correlation diagram. Figure 1 shows all 21 eigenvalues for a system of 20 particles in a double well for α ranging from 0 to 5. For this range of α, the tunneling parameters vary from 1 to 0.0067, going from a low barrier to a high barrier, leading to a fragmented condensate with a fixed number of particles in each well. The correlation diagram shows avoided crossings and energy-level merging. As α increases the levels start to get doubly degenerate; at a value of about $\alpha=1.8$, the highest levels are degenerate and all but the ground state is degenerate for higher values of α.

Looking at the coefficients of eigenvectors reveals interesting characteristics of the ground and excited states. Figures 2(a) and 2(b) show the coefficients of the eigenvectors for the two lowest-lying states for 40 particles for $\alpha=4$. The lowest delocalized states appear to be like the coordinate space wave functions of a harmonic oscillator. These are the states that are below the crossover ridge in a correlation diagram as in Fig. 1. For states over the ridge, a similar list of coefficients for two higher-lying states are shown in Figs. 2(c) and 2(d). These do not look like the harmonic oscillator wave functions. These are examples of states that are superpositions of a macroscopic number of particles on left and right well. For these nearly degenerate Schrödinger cat–like even and odd states, a very high-precision arithmetic is required to get the coefficients.

III. QUANTUM MECHANICAL PHASE-SPACE ANALYSIS

A. Classical Hamiltonian

The classical Hamiltonian that describes the mean-field dynamics of BEC in a double well has been analyzed in several papers [10,22]. In a mean-field assumption [1] for the two-mode double well, and for large enough N, the operators $\hat{a}_j$ can be replaced by the c numbers $\sqrt{n_j}e^{i\theta_j}$, where $j=L,R$. With this assumption and defining $n=(n_L-n_R)/2$, $\theta=\theta_L-\theta_R$, and starting with our model Hamiltonian Eq. (7) gives the classical Hamiltonian

$$H_{cl} = E_c n^2 - E_J\sqrt{1-\left(\frac{2n}{N}\right)^2}\cos\theta + \frac{E_c}{4}N^2 - \frac{E_c}{2}N + \epsilon_{LL}N_L + \epsilon_{RR}N_R, \tag{10}$$

where $E_c=gT_0$ and $E_J=-N[\epsilon_{LR}+gT_1(N-1)]$. Here n and θ are conjugate variables and the equations of motion are

$$\dot{n} = -E_J\sqrt{1-\left(\frac{2n}{N}\right)^2}\sin\theta, \tag{11}$$

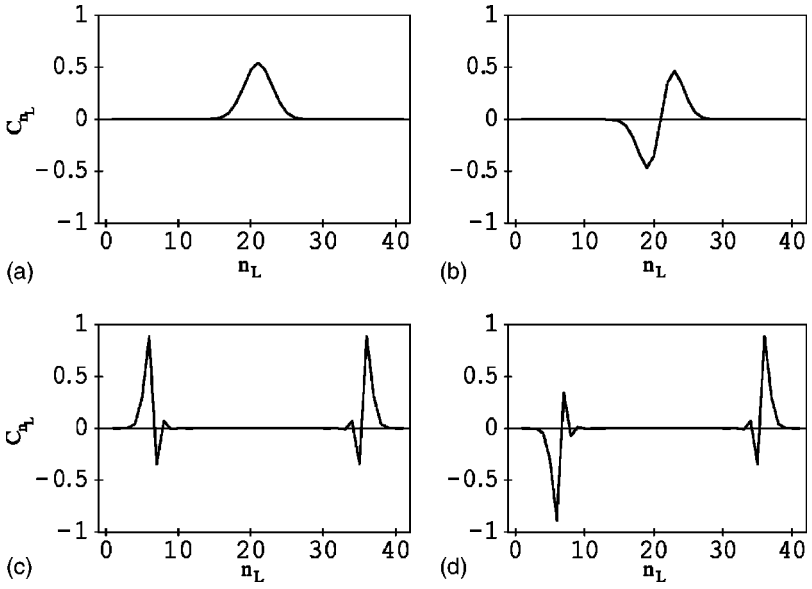

FIG. 2. Fock-state coefficients for $N=40$ for (a) the ground state, (b) the first excited state, (c) the 30th state, and (d) the 31st state. Low-lying states are similar to harmonic-oscillator wave functions, whereas the higher-lying states are macroscopic quantum superpositions of particles simultaneously in both wells.

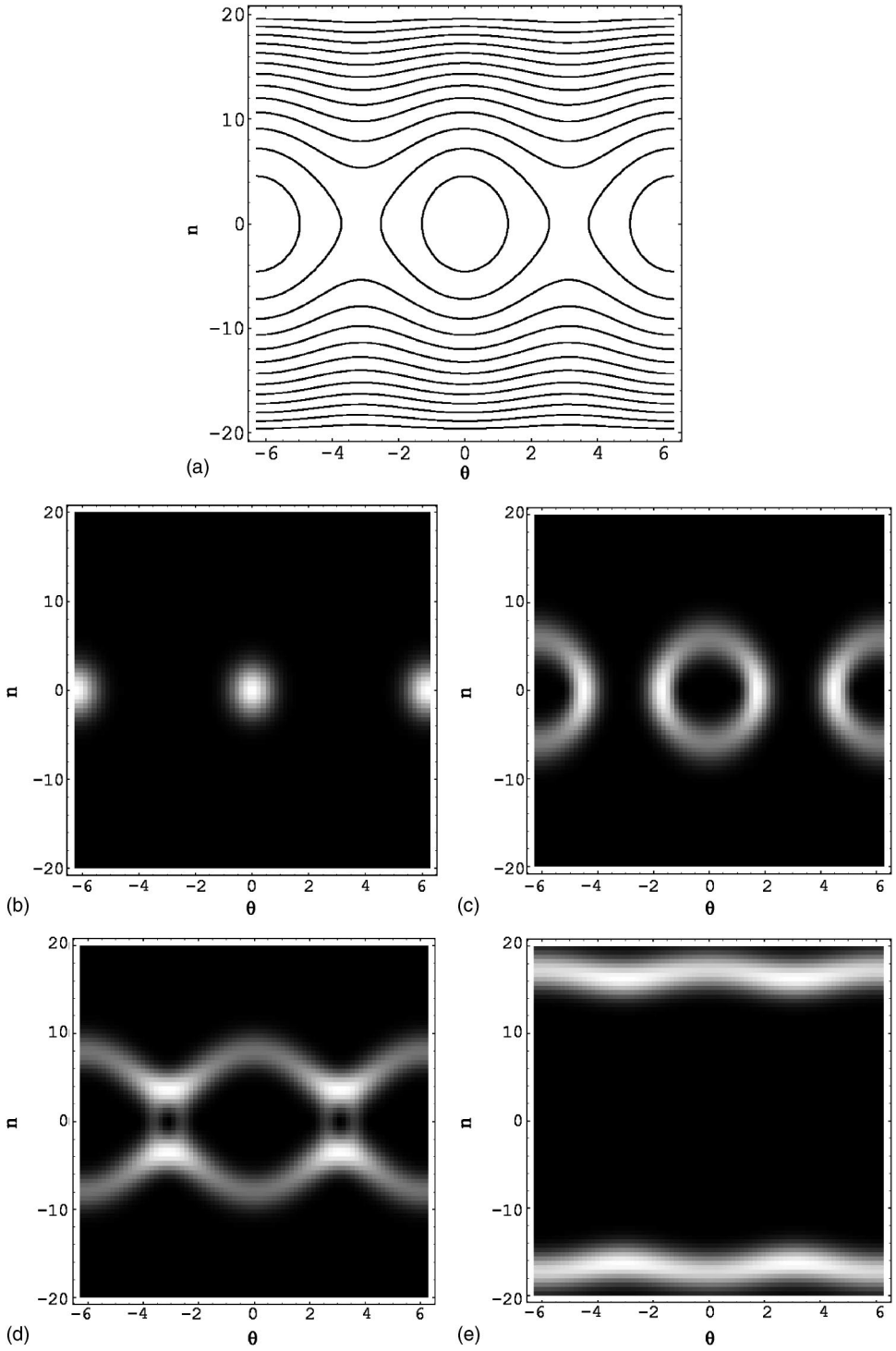

FIG. 3. Comparison of the classical nonrigid physical pendulum phase space with the Husimi distributions for different energy eigenstates for 40 particles. Shown are (a) classical energy contour. Husimi projections for (b) ground state, (c) 6th, (d) 12th, and (e) 35th state.

$$\dot{\theta} = 2E_c n + \frac{4E_J n}{N^2\sqrt{1-\left(\frac{2n}{N}\right)^2}}\cos\theta. \tag{12}$$

Equation (10) is the Hamiltonian of a nonrigid physical pendulum, where θ and n are the angle and angular momentum of the pendulum. The phase space of a nonrigid physical pendulum allows different dynamical regimes, such as the macroscopic quantum self-trapping (MQST) and π motions [13]. MQST refers to the incomplete oscillations of the populations between the two wells. π motion refers to oscillations such that the average relative phase remains π.

B. Husimi distribution function

Since the phase-space distribution function allows one to describe the quantum aspects of a system with as much classical language allowed, it is a popular tool to study semiclassical physics. Among the most popular distribution functions

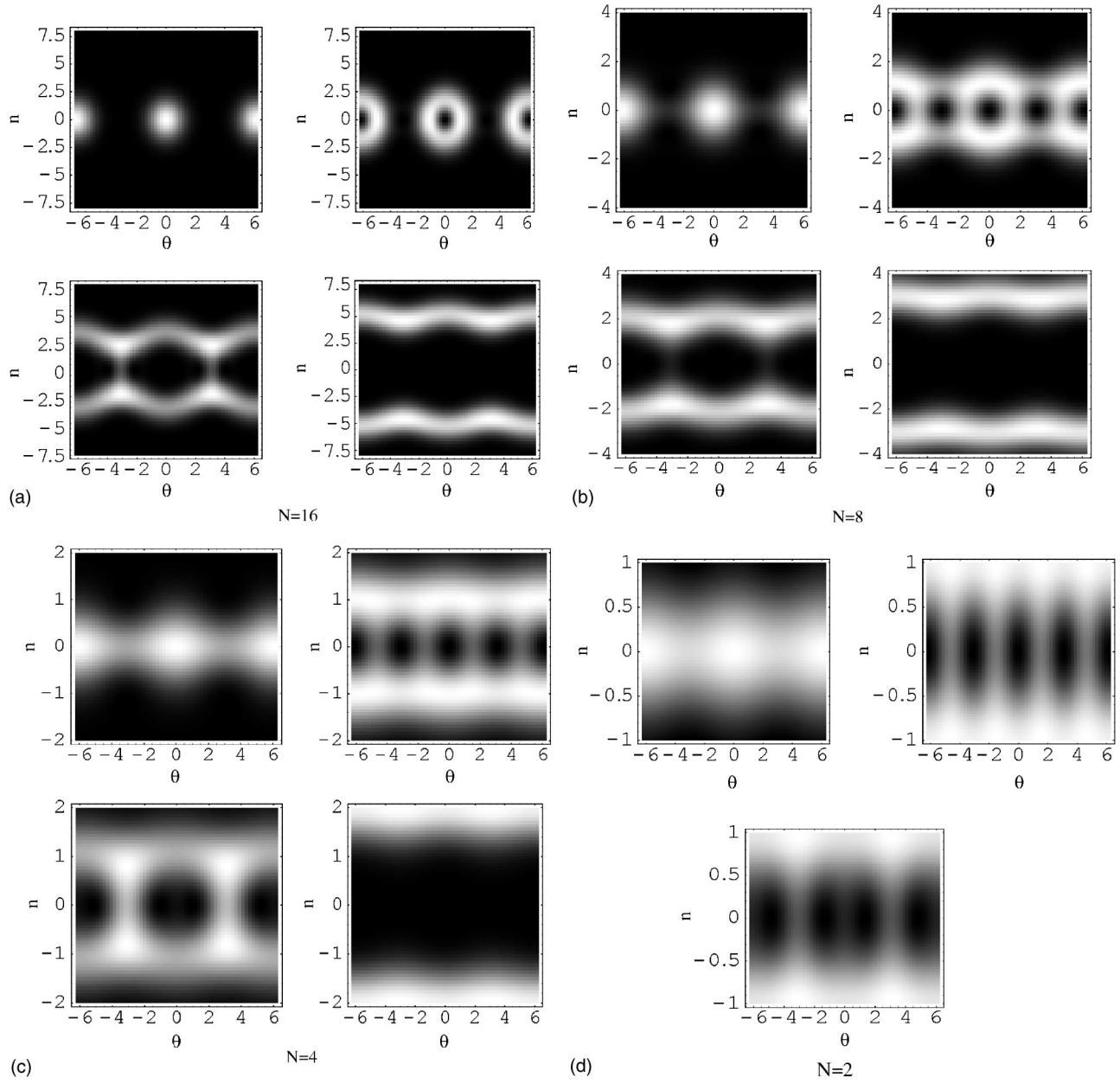

FIG. 4. Quantum-classical correspondence in phase space as functions of number of particles. Shown are the ground state, an oscillator state, a state near the separatrix, and an entangled state for particle numbers (a) 16, (b) 8, (c) 4, and (d) 2. A clear signature of classical pendulum phase space is manifest for $N=8$.

used are the Wigner distribution, Husimi distribution, and the Q function [12,23]. They are all related; the Q function is a special case of the Husimi distribution function. The Wigner function can take negative values and exhibits complex patterns due to fast oscillations. A smoothing of the Wigner function with a squeezed Gaussian gives the Husimi distribution [12], which has a much simpler structure, is easier to interpret and, therefore, more useful for the study of quantum classical correspondence as performed in this paper.

Husimi distribution function can be used to project, in a squeezed coherent state representation, the classical (q,p) phase space behavior from a stationary quantum wave function. Coherent state representation of the electromagnetic field, where n and θ are conjugate variables corresponding to the number and phase of the electromagnetic fields, were discussed by Loudon [24]. The (q,p) coherent state [25] is defined as

$$|\beta\rangle = e^{(-|\beta|^2/2)} \sum_{n'=0}^{\infty} \frac{\beta^{n'}}{\sqrt{n'!}} |n'\rangle, \tag{13}$$

which is a superposition of the harmonic-oscillator eigenstates $|n'\rangle$, here $\beta=q+ip$. For BEC in a double well, the phase difference $\theta=\theta_L-\theta_R$ and the number difference $n=(n_L-n_R)/2$ are the conjugate variable analogous to q and p,

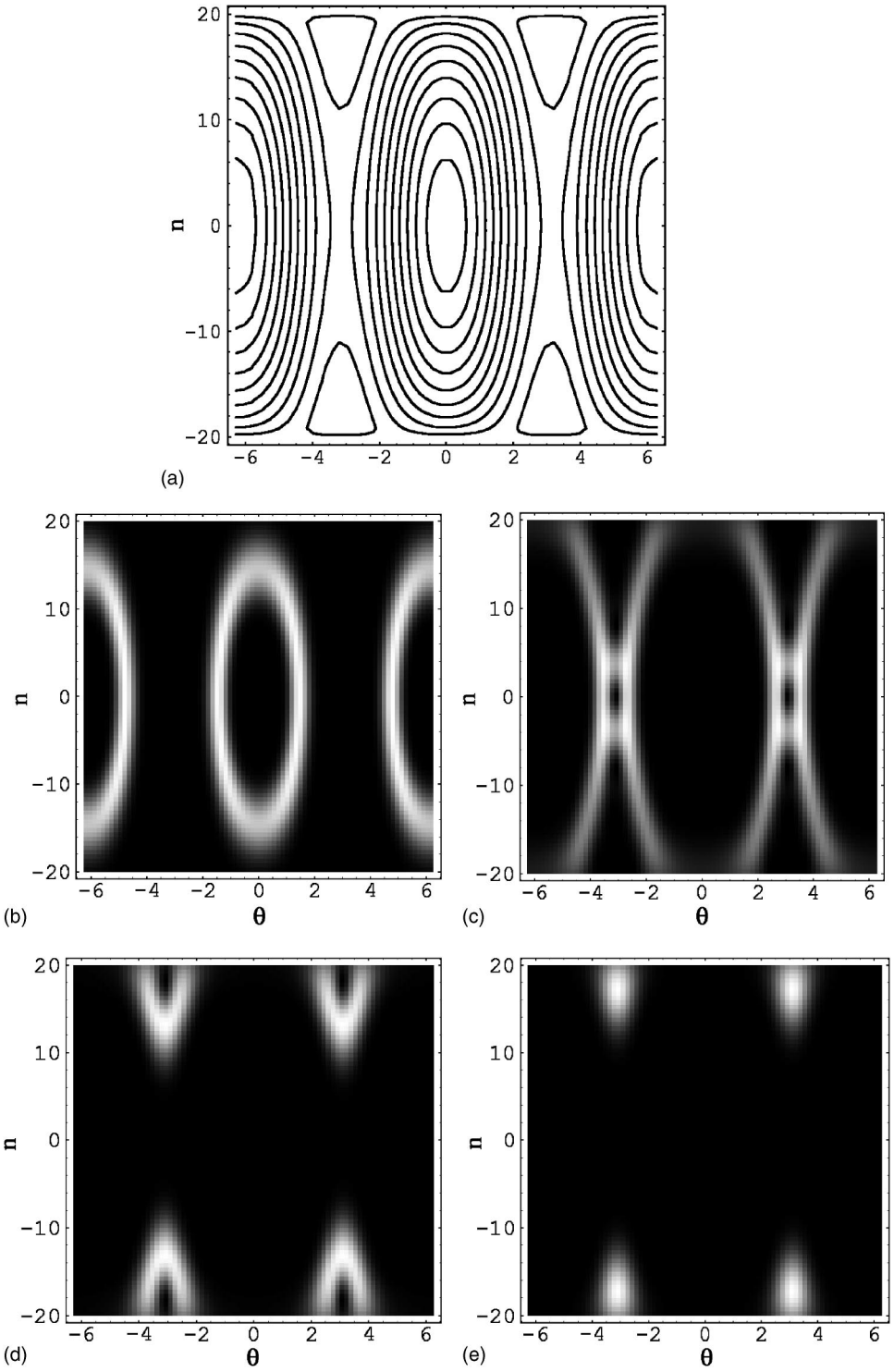

FIG. 5. Comparison of the classical and quantum phase space for $N=40$ showing the analog of π states in the exact quantum treatment. Shown are (a) classical energy contour. Husimi projections are for (b) 12th, (c) 30th, (d) 34th, and (e) 41st states. (d) and (e) are the analogs self-trapped π states of mean-field theory; the quantum states here preserve parity.

respectively. Therefore, in (n,θ) representations, the coordinate and momentum representations of a squeezed coherent state is

$$\langle \theta' | \theta + in \rangle = \frac{1}{(\pi\kappa)^{1/4}} \exp\left[- in\theta' - \frac{(\theta' - \theta)^2}{2\kappa} \right], \quad (14)$$

$$\langle n' | \theta + in \rangle = \frac{1}{(\pi\kappa)^{1/4}} \exp\left[- i\theta n' - \frac{(n' - n)^2}{2\kappa} \right]. \quad (15)$$

In this representation a probability distribution function can be defined as

$$P_j(n,\theta) = |\langle \theta + in | \Psi_j \rangle|^2, \quad (16)$$

where

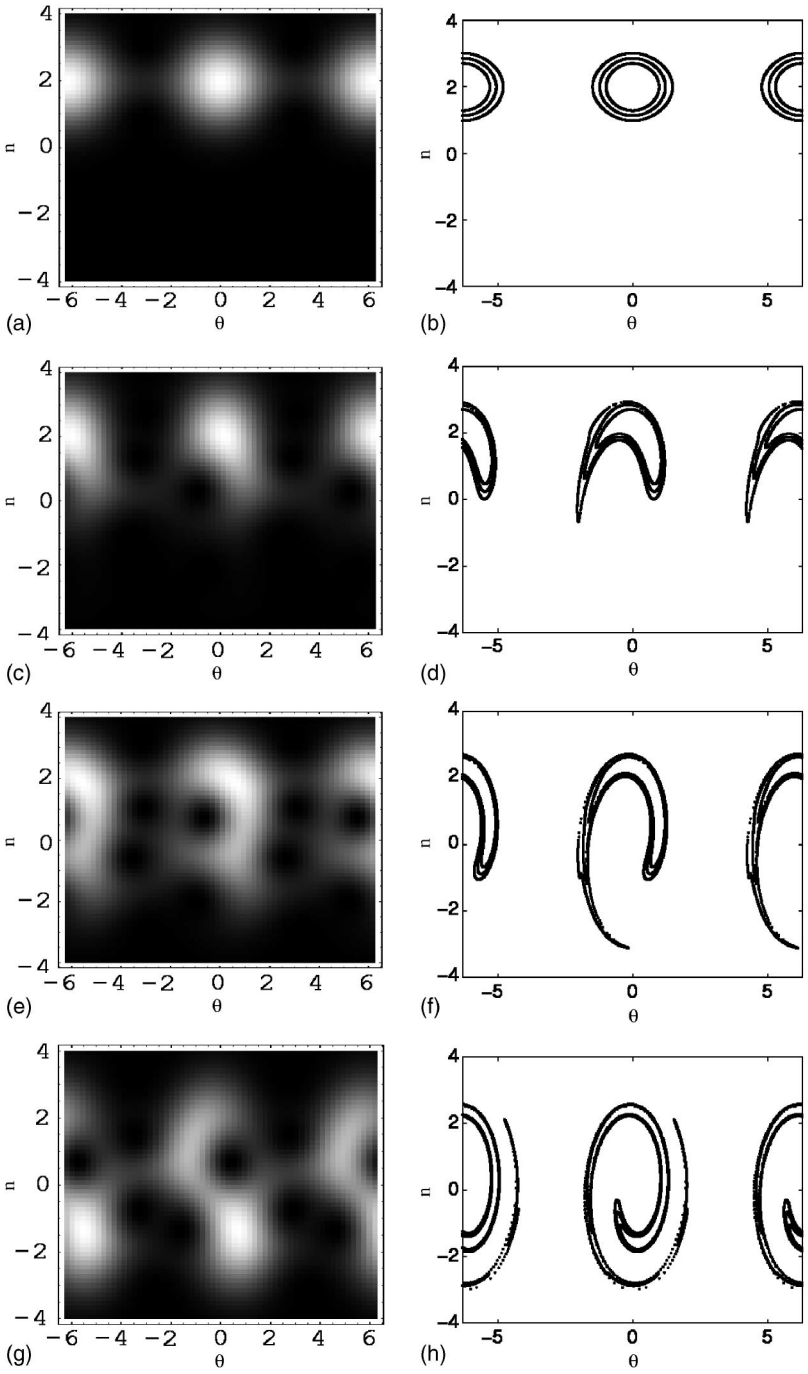

FIG. 6. A comparison of quantum and classical dynamics for $N=8$. We see that the classical points very closely follow the quantum phase-space density. The panels are for (a) initially, and after (b) the first cycle, (c) second cycle, and (d) fourth cycles. The quantum interference effects for shorter times seem to have localizing effects in the region with high density of classical whorls [(g) and (h)]. For much longer times, quantum dynamics shows recurrences as in Fig. 7.

$$\langle \theta + in | \Psi_j \rangle = \frac{1}{(\pi\kappa)^{1/4}} \sum_{n'=-N/2}^{N/2} c_{n'}^{j} \exp\left[i\theta n' - \frac{(n'-n)^2}{2\kappa} \right]. \tag{17}$$

Here $n' = (n_L - n_R)/2$, rather than being the simpler left particle counter, and $c_{n'}$ is the corresponding Fock-state coefficient. Husimi function is defined for any value of the squeezing parameter κ. The Q function in quantum optics is a special case of the Husimi distribution function whenever $\kappa = \omega$, where ω is the frequency of a coherent state Gaussian wave packet [12]. Here $\kappa \approx s\sqrt{2gT_0N(-\epsilon_{12} - gT_1N)}$. s is the inverse squeezing parameter, which is to be determined after looking at the ground state. It is the ratio of the number spread of the ground state of the system to a binomial distribution state. The "coarse-graining" parameter κ determines the relative resolution in phase space in the conjugate variables number and phase. Although the Husimi distribution is defined for any value of the parameter κ [12], taking into account the correct squeezing factor is necessary to obtain quantum-classical correspondence. Otherwise the Husimi projections may have too large a spread in the number or phase variables.

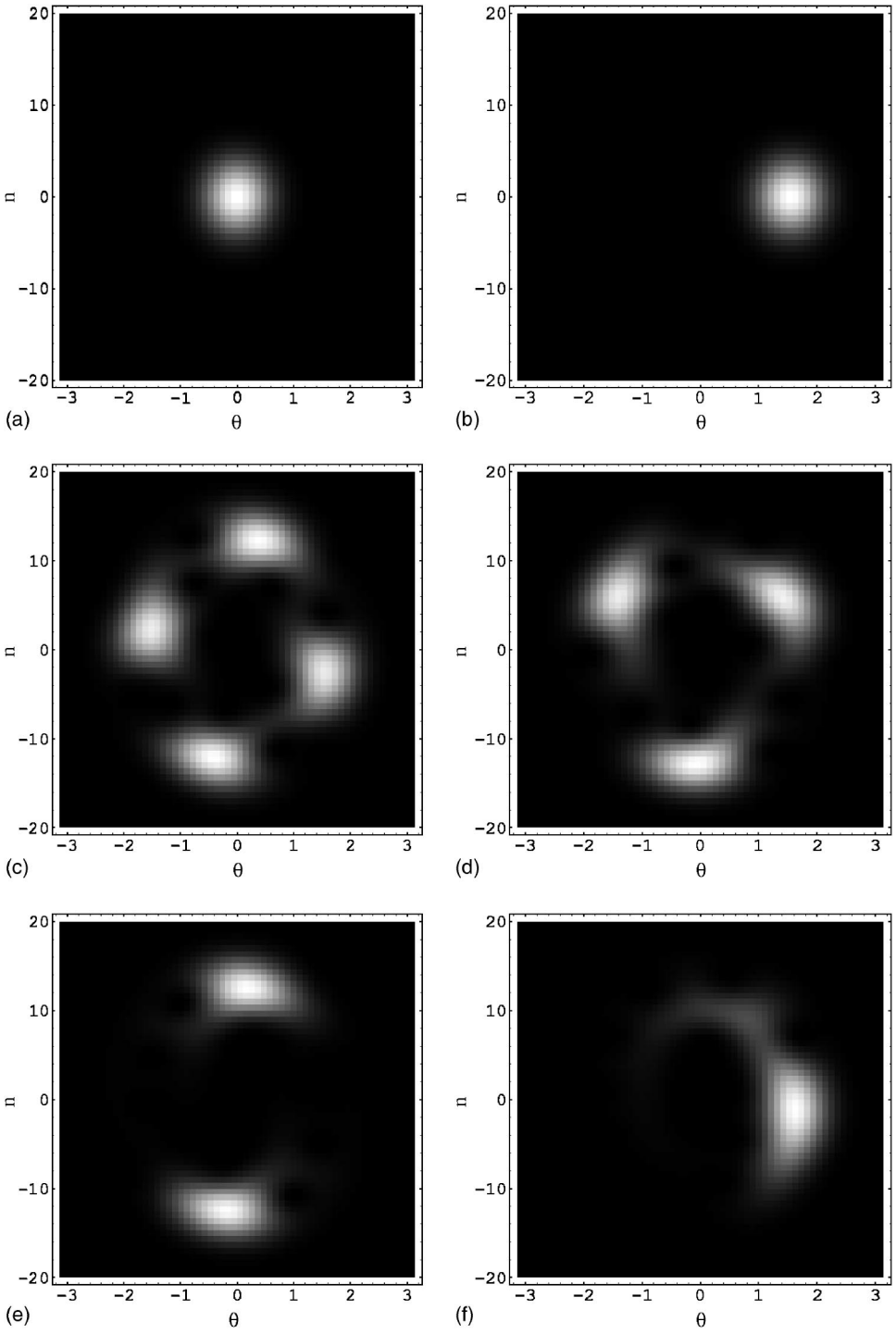

FIG. 7. Husimi projections showing fractional revivals in the dynamics of a phase-displaced ground state for $N=40$. The recurrence time here is $T=12.375$. The panels show (a) ground state, (b) ground state phase displaced by $\pi/2$, and revivals approximately at (c) $T/4$, (d) $T/3$, (e) $T/2$, and (f) T. (e) is an example of a macroscopic superposition of two coherent states, and (f) is approximately a full revival of (b).

C. Quantum-classical connection for the eigenstates

It is natural to ask what aspects of the mean-field phase-space properties of a nonrigid physical pendulum [10] are contained in the exact quantum treatment. We explore that question here by investigating the ground and excited states of the two-mode quantum Hamiltonian and extracting phase-space information through the use of the Husimi distribution function. Figure 3(a) shows the classical energy contours for 40 particles for parameter values $\alpha=4$, $g=1$, and $T_0=1$. For these same parameters, Figs. 3(b)–3(e) show the Husimi distributions for the ground state, 6th, 12th, and 35th states, respectively. The Husimi projections confirm the physical pendulum characteristics of the eigenstates. As is evident from the panels, the ground state is a minimum uncertainty wave packet in both number and phase that is centered at the origin, the harmonic-oscillator-like low-lying excited states are the analog of pendulum librations, and the higher-lying cat–like states are the analog of pendulum rotor motions, with a clear signature of the quantum separatrix state where the libration and rotation states separate.

A systematic exploration is made of the quantum-classical correspondence in phase space for different number of par-

ticles. Figures 4(a)–4(d) show the Husimi distribution for $N=16,8,4,2$, respectively. For each of the particle numbers, it shows the ground state, a low-lying oscillator state, a higher-lying separatrix state, and a macroscopic superposition state. Although the classical energy contours [as shown in Fig. 3(a)] are the same for all different particle numbers, we see here that for $N=4$ and $N=2$ the minimum uncertainty spread of the eigenstates blur the clear signature of a pendulum phase-space structure. It is interesting to note that only four particles per well are needed to reach the semiclassical limit where the classical phase-space structure is evident. By the semiclassical limit here we mean the large N limit where quantum mechanics is approaching the classical. For a very large number of particles the Husimi distributions of the eigenstates become sharper, approaching the classical limit of a line trajectory.

A fundamental difference between the classical trajectories and the quantum states is visible in the rotor state in Fig. 3(e), which is a superposition of most particles in the left and right wells. In the classical sense this corresponds to two different trajectories corresponding to rotor motions of a physical pendulum in two opposite directions. The quantum states always maintain the parity of the Hamiltonian and, hence, the combinations of two such classical trajectories make up a quantum state. The localized motion corresponding to one classical trajectory is known as macroscopic quantum self-trapping (MQST) [10]. Such parity-violating states also appear as stationary solutions of the Gross-Pitaevskii equation in a double well [26].

In order for the quantum Hamiltonian to correspond to a momentum-shortened physical pendulum, there should exist π-type motions [10] among the quantum states. A change in the parameters to $\alpha=4$, $g=0.1$, and $T_0=0.1$ puts us in a slightly different regime, as in Fig. 5(a) showing dynamical regimes with an average phase difference of π. The Husimi projections in Figs. 5(b)–5(e) are, respectively, for the 12th, 30th, 34th, and the 41st states. Here the higher-lying quantum states are the analog of π motions of the mean-field classical Hamiltonian. Again only 4–8 particles per well are needed to reach the semiclassical limit.

IV. DYNAMICS IN PHASE SPACE

A. Comparison of classical and quantum dynamics

To illustrate the applications of the quantum phase-space picture, here we make a comparison of the quantum and classical phase-space dynamics. Investigation of the quantum-classical correspondence in phase space by approximating a Gaussian wave packet with a swarm of points in the classial phase space, although widespread in quantum chaos literature, has not been performed for BEC. This type of comparison between nonaveraged quantities contains the maximum amount of information allowed. By approximating the quantum wave packet with a swarm of points in the classical phase space, the mean-field and quantum dynamics is compared for eight particles in Fig. 6. The first column shows the quantum dynamics in Husimi projection space for a $N/4$ displaced wave packet for $\alpha=4$, and the second column shows the corresponding classical points initially, after the first, second, and fourth cycles, respectively. The effects of dephasing is apparent in the quantum phase space in Figs. 6(e) and 6(g). The classical trajectories develop a narrow whorl-type structure as shown in Figs. 6(f) and 6(h). Surprisingly, even for such a small number of particles, the classical and quantum dynamics is comparable; the quantum states are localized in the region of the classical points with high phase-space density. For a longer time scale the whorls become more convoluted and finer, and the quantum dynamics shows prominent interference effects, such as recurrences, as discussed next.

Schrödinger [27] first pointed out that quantum time evolution of a displaced harmonic-oscillator ground state led to a minimum uncertainty wave packet, which evolves, in time, following its classical phase-space trajectory without any spreading. In the nonlinear pendulum considered here, a ground state displaced by a small amount will evolve in phase space without much spreading. However a state that is farther from the origin will show the effects of nonlinearity and quantum interference a lot quicker. After the full delocalization occurs, the interference effects become pronounced for longer times. Localized peaks appear, which again delocalize with the appearance of new peaks. Figure 7 shows such fractional revivals [28,29] in the Husimi projection space for $N=40$ and $\alpha=2$. For a nonlinear pendulum, as in our model, the revival time has a nontrivial dependence on the various parameters and the initial displacements in phase space. The periods up to various orders for a similar quantum pendulum is given in Ref. [30].

B. Quantum-classical correspondence for classically chaotic dynamics

In the context of chaotic dynamics in BEC, dynamical tunneling of ultracold atoms from a BEC in a modulated

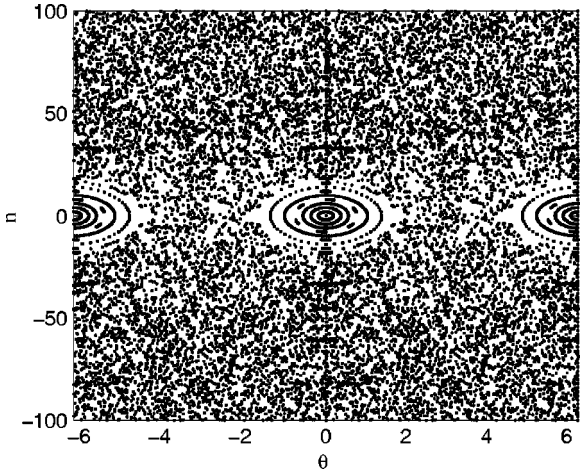

FIG. 8. A composite Poincaré surface of section for 100 trajectories evenly spaced on $\theta=0$. This is for $N=200$ and for a sinusoidal barrier $\alpha=2.5+2.5\,\mathrm{Cos}(10t)$.

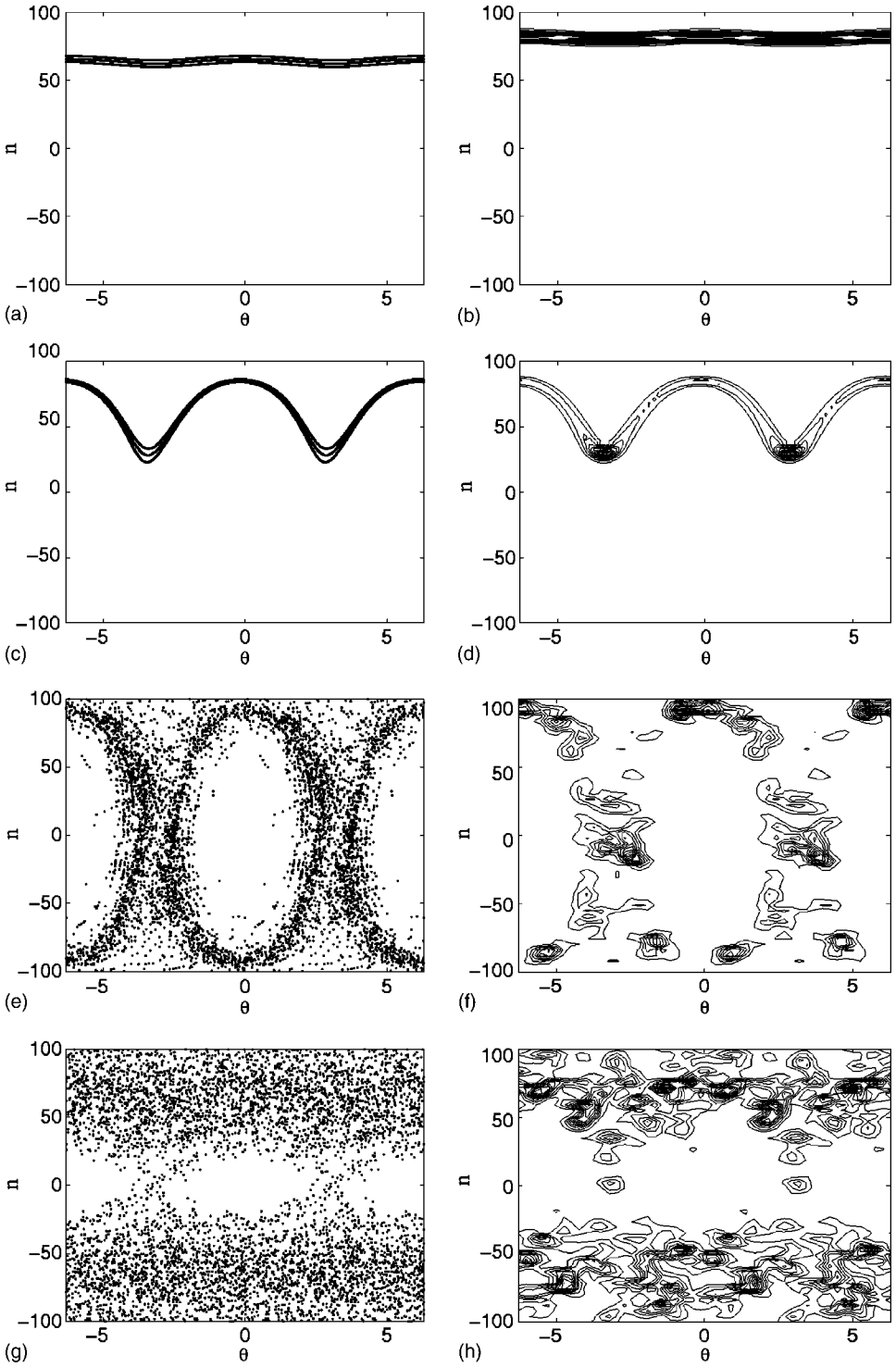

FIG. 9. Comparison of classical and quantum dynamics for points in the chaotic regions of phase space for $N=200$. Right panels show Husimi projections for the time evolution of the localized superposition of 128th and 129th eigenstates and the left panels show the time evolution of three bands of classical trajectories intially localized in the same region. (a),(b) at $t=0$; (c),(d) $t=0.17$; (e),(f) $t=1.7$; and (g),(h) $t=5$. Quantum states are visibly localized around the chaotic classical points.

periodic potential has been observed [13], and a theoretical study of a similar system has been done using the Floquet operator [14]. These authors showed that exact quantum dynamics of the system can exhibit classically forbidden tunneling between two regular regions in the corresponding classical phase space, a phenomenon known as dynamical tunneling [31]. Here we study instead the similarities in the dynamics in the classical and quantum phase space. A driven pendulum is a well-known example of a one-and-half-degree-of-freedom classical system exhibiting chaos. For an analogous system of a driven double-well BEC, we make a comparison of the quantum states at different times with the corresponding classical trajectories and illustrate signatures of quantum chaos. Such comparison is done in phase space most usefully between the Husimi projection of a quantum state and the corresponding classical band of points initially in the same region of phase space [32]. For a diagnostic to the classical phase space, Fig. 8 shows the Poincaré section

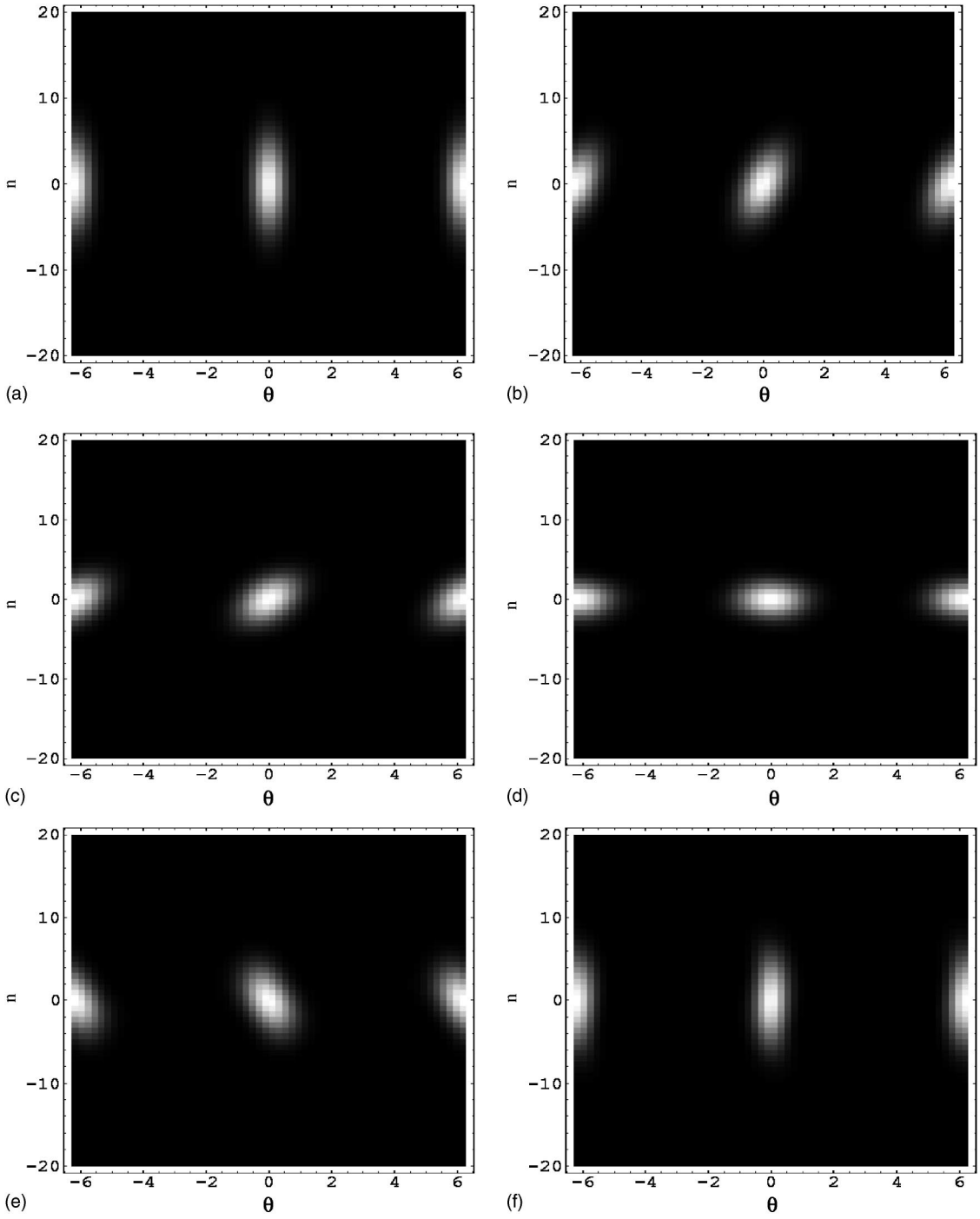

FIG. 10. Husimi projections showing rotations in phase space for $N=40$. (a) The initial phase-squeezed or coherent state at $t=0$, (b) slightly rotated state at $t=0.075$, (c) $t=0.09$, (d) at $t=0.125$, a number-squeezed state, (e) $t=0.165$, (f) at $t=0.25$ the evolution brings the state back to the initial phase-squeezed state.

for 200 particles and $\alpha=2.5+2.5\cos(10t)$. As the amplitude of the driving force becomes larger the whole phase space becomes chaotic.

For comparisons in the chaotic region, the Husimi distribution of the superpositions of 128th and 129th eigenstates at different times are shown in Figs. 9(b), 9(d), 9(f), and 9(h). The classical trajectories of similar points are shown in Figs. 9(a), 9(c), 9(e), and 9(g). At shorter time $t=0.17$ as shown in Figs. 9(c) and 9(d), the quantum state very nicely follows the classical points. Figures 9(e) and 9(f) are a comparison for points showing a visibly chaotic yet localized pattern both in the classical and quantum phase space. The effect of chaotic dynamics fully takes effect at $t=5$ when the classical phase-space points are diffused throughout the whole region as shown in Fig. 9(g). A comparison with the Husimi projections in Fig. 9(h) makes evident the manifestations of chaos

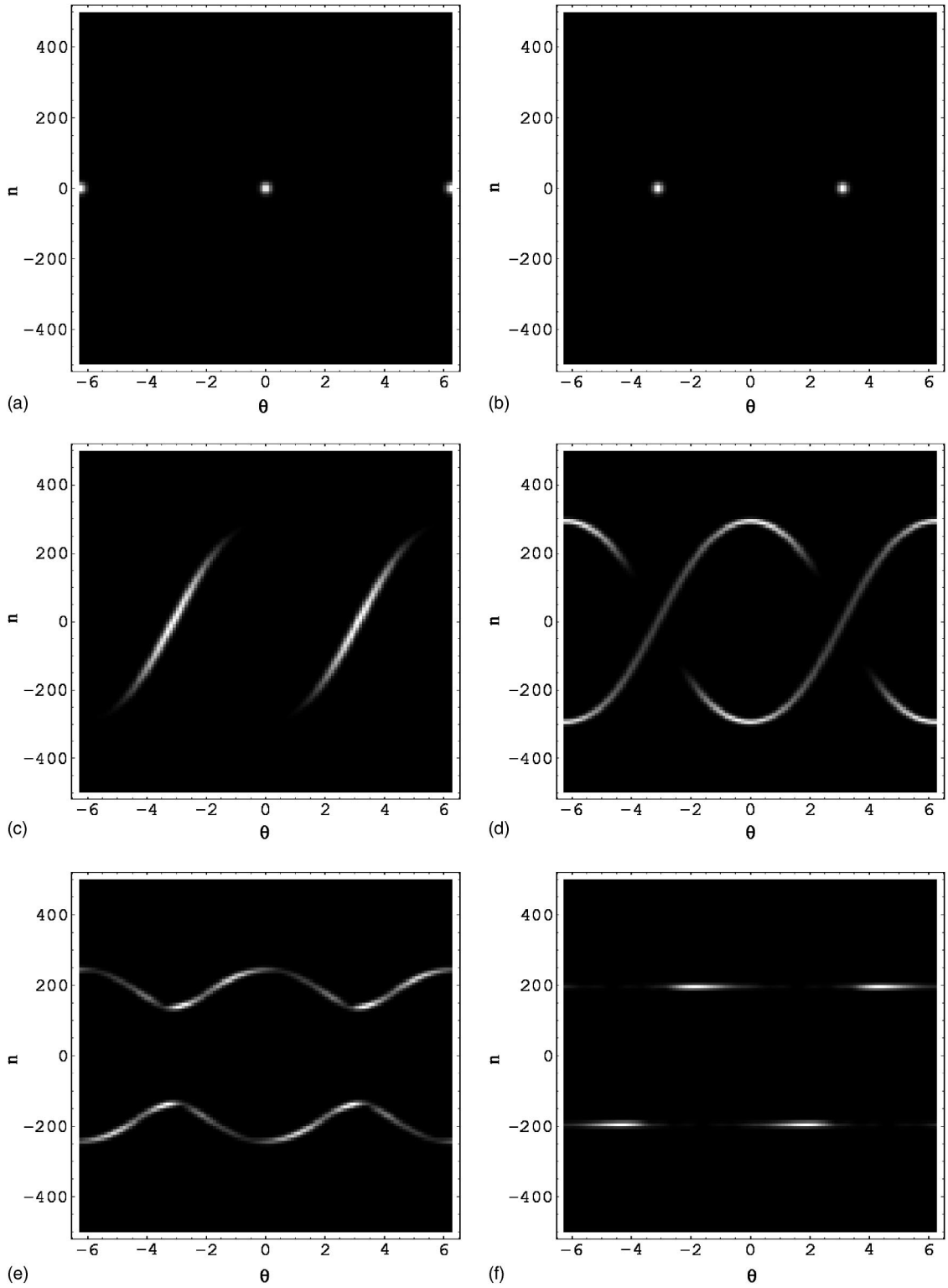

FIG. 11. Shown is the evolution to an entangled state of $N=1000$ in Husimi projection space. (a) The ground state at $t=0$, (b) the π-phase imprinted ground state at the hyperbolic fixed point, (c) at $t=0.01$ the wave packet is bifurcating along the separatrix, (d) at $t=0.016$ it continues to move along the separatrix, (e) at $t=0.4$ the states become trapped as we increase the barrier, and (f) at $t=2.3$ a sharply peaked entangled state is obtained.

in the quantum dynamics. A state initially localized in the regular regions of phase space does not give rise to such chaotic structures. In the limit when $\hbar \to 0$ or equivalently $1/N \to 0$, the discrete quantum energy spectrum becomes continuous and the quantum mechanics will more closely follow classical mechanics; any evidence of chaos in the quantum dynamics will be better represented in such comparisons.

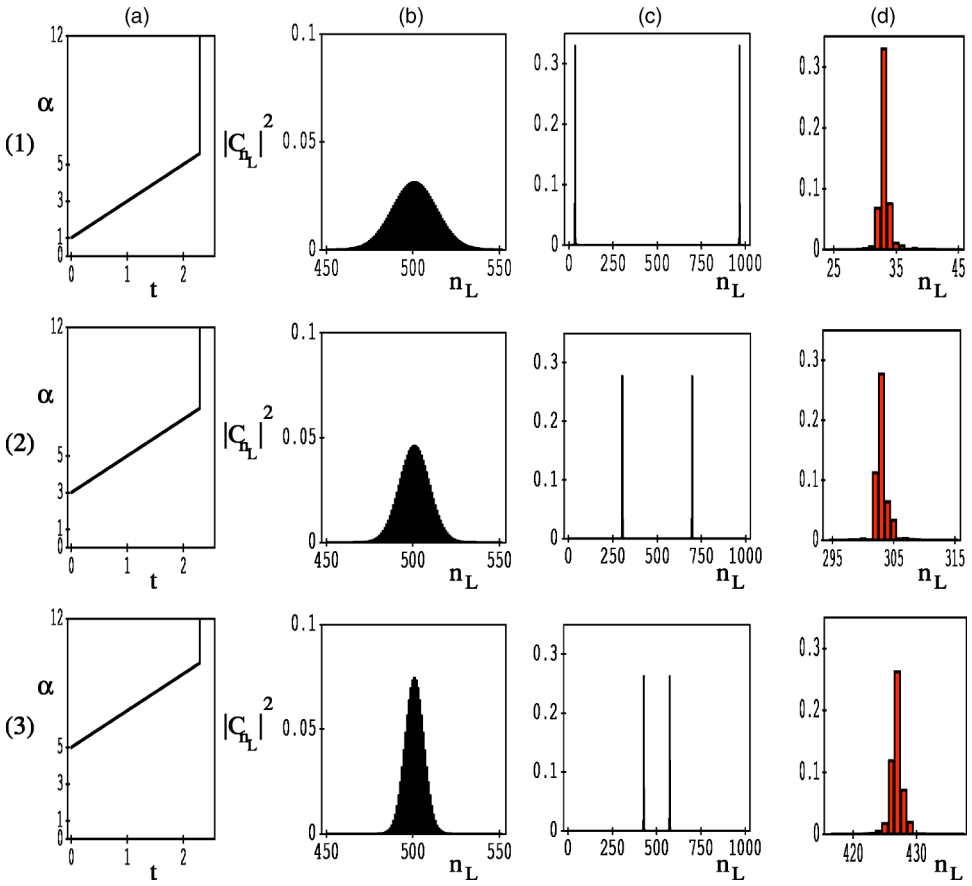

FIG. 12. Shown are the entangled states for $N=1000$ with different initial heights of the barrier and, therefore, different initial squeezings of the BEC ground state, but the same ramping of the potential. Row (1) shows the states where $\alpha=1+2t$: (a) the parameter α as a function of time, (b) the ground state, (c) the final entangled state, and (d) a magnified view of the Fock-state coefficients. Rows (2) and (3) show the results for $\alpha=3+2t$ and $\alpha=5+2t$, respectively. The initial barrier height controls the extremity of the entangled states. Note that for clarity the axes in the panels have different scalings.

C. Relative number and phase squeezing

Ground-state number squeezing with a variable barrier height in double and multiwell systems has been discussed and observed by many authors [2,3,5]. The case of a sudden change of barrier height on a coherent ground state, which we analyze here, has been discussed on a theoretical basis [2,15]. In Ref. [15], the authors consider the evolution, in the space of number differences, of an intially perfect binomial number distribution state, and find that for an optimal value of parameters in the Hamiltonian, the initial state periodically evolves to a relatively number-squeezed state.

We perform here a quantum phase-space analysis of this phenomenon and find this to be a property of coherent ground state evolving under a Hamiltonian for which it is not an eigenstate. We show that the initial state rotates in the number-angle phase space and thus becomes elongated or well defined in number and phase periodically. We illustrate this with an example: the ground state for $\alpha=0$ very closely approximates a state with a binomial distribution of Fock-state coefficients. With a sudden raising of the barrier to $\alpha=3$, we follow the evolution of the state in phase space. The initial coherent ground state is not an eigenstate of the changed potential and hence will time evolve accordingly. As shown in the quantum phase space in Fig. 10(a), the initial state is rather well defined in phase (θ) and elongated in number difference (n). Further evolution in the new potential rotates the elongation in phase space such that after a certain period it becomes well defined in n [as in Fig. 10(d)] or it is relatively number squeezed. A full cycle is shown in Fig. 10; in Fig. 10(f) the evolution brings it back to the initial coherent state. The period, for a linearized system of equations of the pendulum is given by $2\pi/\sqrt{2E_CE_J+4E_J^2/N^2}$.

V. GENERATING TUNABLE ENTANGLED STATES USING PHASE ENGINEERING

The quantum phase-space model presented here points to a simple way that an entangled state can be generated with a single-component BEC in a double well. A wave-packet π phase displaced to the unstable hyperbolic fixed point of a classical phase space bifurcates along the separatrix if allowed to time evolve. With the above motivation, here we provide a visual explanation in phase space of the creation of controlled entangled number states of a BEC in a double well via phase imprinting on the part of the condensate in one of the wells followed by a continuous change of barrier height. When properly implemented this results in a state of the form

$$|\Psi\rangle = \frac{1}{\sqrt{2}}(|n_L, N-n_L\rangle + |N-n_L, n_L\rangle), \tag{18}$$

where $|n_L, n_R\rangle$ denotes a state with n_L particles in the left well, n_R in the right well, and with total number of particles $N=n_L+n_R$. Unlike in other proposals [17–20], we can use the barrier height to control the squeezing of the initial BEC ground state followed by a continuous change of barrier height to control both the extremity [the value of n_L (n_L

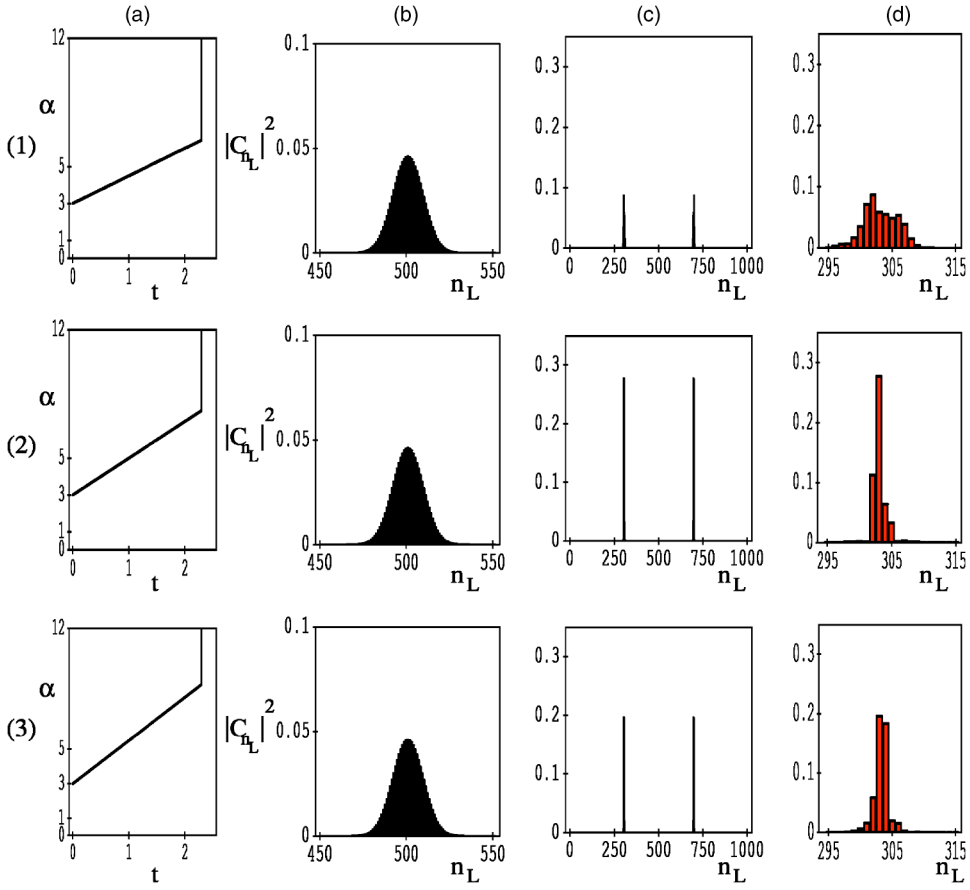

FIG. 13. Shown are the entangled states for $N=1000$ with same initial squeezings of the BEC ground state, but different ramping of the potential. Row (1) shows the states where $\alpha=3+1.5t$: (a) the parameter α as a function of time (note different ramping); (b) the ground state, the initial states are the same; (c) the final entangled state, and (d) a magnified view of the Fock-state coefficients. Rows (2) and (3) show the results for $\alpha=3+2t$ and $\alpha=3+2.5t$, respectively. The ramping rate controls the sharpness of the entangled states.

$=0,1,2,\ldots,N)$] and the sharpness (the spread around n_L) of the entangled state. An extreme entangled state would correspond to $n_L=0$ or N.

Writing phases on part of a condensate is experimentally feasible via interaction with a far off-resonance laser. This method has been used to generate dark solitons and measure their velocities due to a phase offset [33]. Mathematically, such a method corresponds to multiplying the coefficient of each of the Fock states in the expansion of an eigenstate by $e^{in_L\theta}$, where $|n_L\rangle$ is the corresponding Fock state and θ is the phase offset for particles in the left well. By π phase imprinting the condensate in one well, the ground state centered at the origin (0,0) in phase space is displaced to the unstable equilibrium point $(0,\pi)$ on the separatrix. Using exact quantum time evolution within the framework of the two-mode model, the resulting quantum wave packet bifurcates as expected. If the barrier is raised as discussed below, then the wave packet is permanently split, resulting in a superposition of two classical rotor states.

A. Entangled state generation without decoherence

In the situation when there is no decoherence, well-controlled entangled states can be generated within the two-mode quantum dynamics. As an example, Fig. 11 shows how a number-entangled state with 1000 particles is generated. Figure 11 also shows the evolution in phase space using Husimi projections: (a) the ground state, (b) a π-phase imprinted state, and (c) and (d) show subsequent evolution in the process of bifurcating the state. Further evolution along with a change of barrier totally splits and traps the state symmetrically above the separatrix, as shown in Fig. 11(e), finally giving rise to an entangled state in Fig. 11(f) at $t=2.3$. Here the barrier height is ramped up in time as $\alpha=3+2t$. When an entangled state is reached the barrier is suddenly raised to essentially halt the evolution. With different initial barrier heights and the same ramping of the potential, the extremity of the entangled states can be tuned. Examples are shown in Fig. 12 where the different values of the barrier heights are $\alpha=1+2t$, $\alpha=3+2t$, and $\alpha=5+2t$ for rows (1), (2), and (3), respectively. The columns in Fig. 12 show: (a) the barrier height and the ramping, (b) the respective ground state, (c) the final entangled state at the end of the ramping, and (d) a close view of the coefficients for the final state, which shows that these are rather sharply peaked entangled states. As is evident from the pictures, the initial squeezing of the ground state determines the extremity of the final entangled state. Here we choose to show snapshots of the final states for different barrier heights at the same unitless time $t=2.3$. In the phase-space picture, this is the approximate time it takes the wave-packet points on the unstable fixed point to reach the top of the separatrix, the farthest in number distribution. The velocity of wave-packet points along the phase-space trajectory is faster for an initial low barrier compared to an initial high barrier; however, the distance traveled is greater. Thus although nonlinear dynamics is responsible for the classical time evolution, the time to reach a good entangled state is independent of barrier height in our

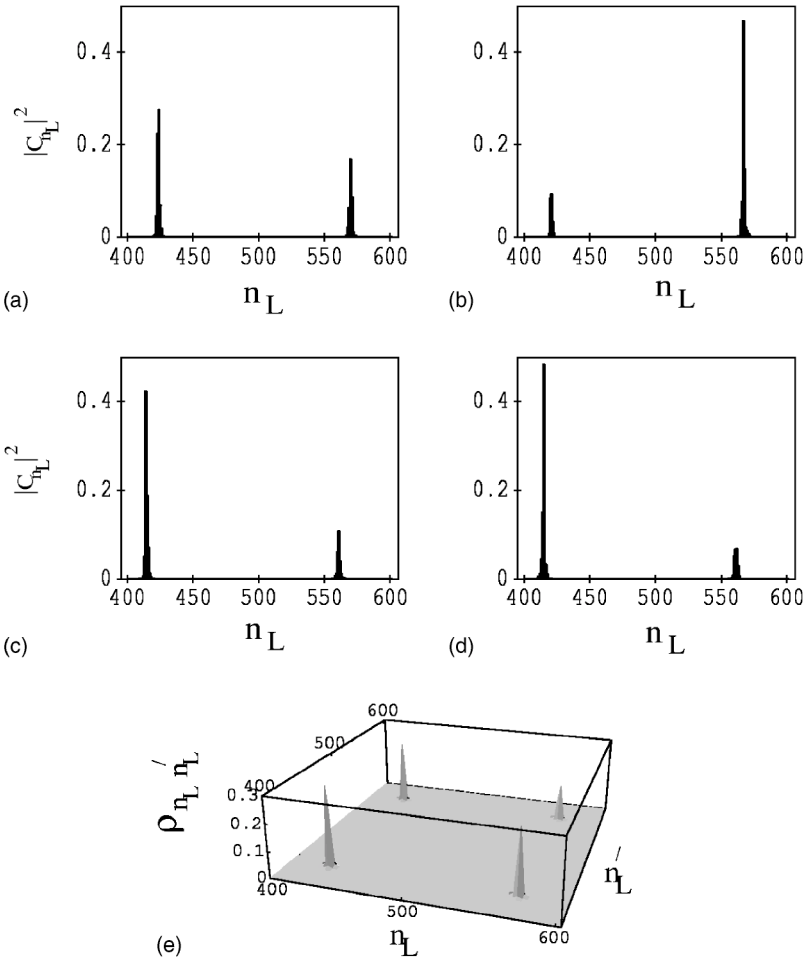

FIG. 14. Effects of loss of particles on entangled states. (a) and (b) show the effect of loss of 10 particles on the less extreme entangled state example of the third row in Fig. 13. (c) and (d) show the effects of loss of 30 particles. (e) shows density matrix for panel (a), indicating that the coherence is not lost.

simulations. For the same initial barrier height (same initial squeezing), a different barrier ramping rate can be used to generate final superposition states with differing sharpness. This is shown in Fig. 13 where different barrier ramping is used for each row resulting in sharply peaked and nonsharp states. Rows (1), (2), and (3) are for $\alpha=3+1.5t$, $\alpha=3+2t$, and $\alpha=3+2.5t$, respectively. Controllability of both extremity and sharpness helps in the generation of robust entangled states as is discussed in Sec. V B

B. Entangled state generation with loss

Macroscopic superposition states are not observed mainly due to interaction with the environment. In elastic collisions where the total number of atom is conserved, phase damping destroys the quantum coherence [34]. In the case where the number of particles are not conserved, the loss of even a single particle destroys an extreme entangled state [18], as can be seen with the operation of a destruction operator to such a state

$$\hat{a}_1(|N,0\rangle + |0,N\rangle)/\sqrt{2} = \sqrt{N/2}|N-1,0\rangle. \tag{19}$$

The robustness of the entangled states is tested with such a loss scheme. It is likely that particles from the condensate will be lost during the evolution of the state when the barrier is raised. This is simulated by the operation of the destruction operator at different time intervals during the evolution and taking particles out randomly from either well at each time. Losses can be due to magnetic field changes, three body recombinations, or Feshbach resonances. The upper limits are 1.6×10^{-16} cm^3/s for the two-body loss rate coefficient and 5.8×10^{-30} cm^6/s for the three-body loss rate coefficient [35,36]. Equation (1) of Ref. [35] can be used to find the loss of particles, which depends on the rate constants, density of atoms, and the volume of the trap. For a density of 5×10^{13} cm^{-3}, a trap of $100\times10\times10$ μ^3 and the upper limit of three-body loss rate mentioned above, seven particles per millisecond are lost from the trap. For a ^{87}Rb condensate, $\lambda=840$ nm, $a_{sc}=5.8$ nm, $\epsilon_{LR}=-0.04E_R e^{-\alpha}$ (E_R is recoil energy from absorption of a photon), and taking $gT_0=0.04E_R$ as approximately constant for calculational purposes, the entangled state in our study is formed at 2.8 ms. This amounts to a loss of 15–20 particles during the formation of the entangled state. Minimal losses can be obtained with optimal choice of parameters. This loss in the number of particles is in addition to the phase damping decoherence mechanisms for which we refer to Ref. [34].

We simulate here the loss of 1–3 % of the condensate particles, which is reasonable. Figure 14 shows different realizations of loss of different number of particles from the least extreme entangled state example in Fig. 12, third row. Figures 14(a) and 14(b) are two different simulations for a loss of 10 particles during the evolution. Figures 14(c) and

14(d) show two different runs for a loss of 30 particles from the same entangled state. Results for extreme entangled states are not shown here as such states are totally destroyed, meaning all the particles are localized in one well. The simulations suggests that a less extreme entangled state is more robust, so it may be desirable to sacrifice the extremity of a cat state in order for it to survive in a realistic laboratory setting. To compare the effects of loss for sharpness, an entangled state, which is not sharp and has a Gaussian spread, has a better chance of having nonvanishing coefficients after the loss of particles. So the most robust state would be a less extreme entangled state with a Gaussian width of coefficients around the two peaks. The coherence is not lost in destroying particles in the fashion done here; this is evident in the density matrix [34] for Fig. 14(a) as shown in Fig. 14(e). The off-diagonal peaks in the density matrix that quantifies the coherence remains a geometric mean of the diagonal elements because we have not introduced phase damping; coherence vanishes only when the final state is localized in one well. In Ref. [33] the authors study dissipation of a dark soliton after a phase imprinting has been applied and for a nonzero temperature. At the higher temperature phase decoherence is rapid. Finite temperature would lead to a serious source of decoherence for the system considered here.

C. Discussions

During our development of the quantum phase-space picture for the double-well BEC since 2002 [11,37], several other authors have also noted that metastable quantum states and dynamical instability can be exploited to produce entangled states in a double well [19] and in a two-component condensate [20]. All these findings are consistent with the phase-space model discussed in this paper; our demonstration of the tunability and sharpening of the entangled states in a double-well setting provides a useful improvement that may be important for experimental detection and other practical purposes. The Wigner distribution function, the Gaussian average of which is the Husimi distribution, has also emerged as a valuable tool for the description of entangled state generation in a two-component condensate [20].

VI. REMARKS AND SUMMARY

We have developed a quantum mechanical phase-space picture of a double-well Bose-Einstein condensate in the two-mode approximation. In a mean-field approximation, the two-mode Hamiltonian reduces to the Hamiltonian of a nonrigid physical pendulum. Examination of the Husimi projections of the stationary quantum states reveals how the mean-field classical phase space follows directly from quantum mechanics. We have found eigenstate structures that are localized, such as classical oscillating, free-rotor, and π states.

The Husimi probability distribution turns out to be an extremely useful tool to study BECs in a double well. Through its study we found unifying connections and insights into the double-well phase space and its dynamics. For a driven double well, quantum states are found to diffuse into the chaotic region of phase space analogous to classical chaos. A π phase imprinted condensate put on an unstable fixed point of the classical phase space bifurcates along the separatrix if allowed to time evolve. The extremity and the sharpness of the entangled states produced in this scheme can be tuned with the initial barrier height and the appropriate ramping of the potential. The model developed here may find applications in the studies of other double-well BEC dynamics, such as in a study of asymmetric wells, effects of change of scattering lengths, transitions connected to avoided crossings, topics in quantum chaos, and studies of the effects of decoherence.

ACKNOWLEDGMENTS

We would like to thank Sarah B. McKinney for discussions and computational support. This work was supported by NSF Grant No. PHY-0140091.

[1] A. J. Leggett, Rev. Mod. Phys. **73**, 307 (2001).
[2] C. Orzel, A. K. Tuchman, M. L. Fensclau, M. Yasuda, and M. A. Kasevich, Science **291**, 2386 (2001).
[3] M. Greiner, O. Mandel, T. Esslinger, T. W. Hansch, and I. Bloch, Nature (London) **415**, 39 (2002).
[4] G. J. Milburn, J. Corney, E. M. Wright, and D. F. Walls, Phys. Rev. A **55**, 4318 (1997).
[5] R. W. Spekkens and J. E. Sipe, Phys. Rev. A **59**, 3868 (1999).
[6] B. Josephson, Phys. Lett. **1**, 251 (1962).
[7] M. R. Andrews, C. G. Townsend, H.-J. Miesner, D. S. Durfee, D. M. Kurn, and W. Ketterle, Science **275**, 637 (1997).
[8] P. W. Anderson, in *Lectures on the Many-Body Problem*, edited by E. R. Caianiello (Academic, New York, 1964), Vol. 2.
[9] D. R. Tilley and J. Tilley, *Superfluidity and Superconductivity* (Institute of Physics, Bristol, 1990).
[10] A. Smerzi, S. Fantoni, S. Giovanazzi, and S. R. Shenoy, Phys. Rev. Lett. **79**, 4950 (1997); S. Raghavan, A. Smerzi, S. Fantoni, and S. R. Shenoy, Phys. Rev. A **59**, 620 (1999).
[11] W. P. Reinhardt and H. Perry, in *Fundamental World in Quantum Chemistry*, edited by E. J. Brandas and E. S. Kryachko (Kluwer, Dordrecht, 2003), Vol. 2, Chap. 12.
[12] K. Husimi, Proc. Physico-Math. Soc. Japan **22**, 264 (1940); H. Lee, Phys. Rep. **259**, 147 (1995).
[13] W. K. Hensinger *et al.*, Nature (London) **412**, 52 (2001).
[14] G. L. Salmond, C. A. Holmes, and G. J. Milburn, Phys. Rev. A **65**, 033623 (2002).
[15] J. A. Dunningham, K. Burnett, and M. Edwards, Phys. Rev. A **64**, 015601 (2001).
[16] J. R. Friedman, V. Patel, W. Chen, S. K. Tolpygo, and J. E. Lukens, Nature (London) **406**, 43 (2000); C. H. van der Wal *et al.*, Science **290**, 773 (2000).
[17] J. I. Cirac, M. Lewenstein, K. Molmer, and P. Zoller, Phys. Rev. A **57**, 1208 (1998); D. Gordon and C. M. Savage, *ibid.* **59**, 4623 (1999).

[18] J. A. Dunningham and K. Burnett, J. Mod. Opt. **48**, 1837 (2001).
[19] A. Polkovnikov, Phys. Rev. A **68**, 033609 (2003); A. Polkovnikov, S. Sachdev, and S. M. Girvin, *ibid.* **66**, 053607 (2002).
[20] A. Micheli, D. Jaksch, J. I. Cirac, and P. Zoller, Phys. Rev. A **67**, 013607 (2003).
[21] M. P. A. Fisher, P. B. Weichman, G. Grinstein, and D. S. Fisher, Phys. Rev. B **40**, 546 (1989).
[22] J. R. Anglin, P. Drummond, and A. Smerzi, Phys. Rev. A **64**, 063605 (2001).
[23] C. W. Gardiner and P. Zoller, *Quantum Noise* (Springer, Berlin, 2000).
[24] R. Loudon, *The Quantum Theory of Light* (Oxford, London, 1973).
[25] A. Perelomov, *Generalized Coherent States and Their Applications* (Springer, Berlin, 1986).
[26] K. W. Mahmud, J. N. Kutz, and W. P. Reinhardt, Phys. Rev. A **66**, 063607 (2002); R. D'Agosta and C. Presilla, *ibid.* **65**, 043609 (2002).
[27] E. Schrödinger, *Collected Papers on Wave Mechanics* (Chelsea, New York, 1982).
[28] E. M. Wright, D. F. Walls, and J. C. Garrison, Phys. Rev. Lett. **77**, 2158 (1996).
[29] M. Greiner, O. Mandel, T. Esslinger, T. W. Hansch, and I. Bloch, Nature (London) **419**, 51 (2002).
[30] J. C. Ross and H. W. Capel, Physica A **77**, 2158 (1996).
[31] M. J. Davis and E. J. Heller, J. Chem. Phys. **75**, 246 (1981).
[32] K. Takahashi, Prog. Theor. Phys. Suppl. **98**, 109 (1989).
[33] J. Denschlag *et al.*, Science **287**, 97 (2000); S. Burger *et al.*, Phys. Rev. Lett. **83**, 5198 (1999).
[34] P. J. Y. Louis, P. M. R. Brydon, and C. M. Savage, Phys. Rev. A **64**, 053613 (2001).
[35] E. A. Burt *et al.*, Phys. Rev. Lett. **79**, 337 (1997).
[36] A. Montina and F. T. Arecchi, Phys. Rev. A **67**, 023616 (2003).
[37] K. W. Mahmud, H. Perry, and W. P. Reinhardt, J. Phys. B **36**, L265 (2003).